Computing Bulk Phase Resonance Raman Spectra from *ab initio* Molecular Dynamics and Real-Time TDDFT

Supporting Information

Martin Brehm* and Martin Thomas

Institut für Chemie - Theoretische Chemie, Martin-Luther-Universität Halle-Wittenberg, Von-Danckelmann-Platz 4, 06120 Halle (Saale), Germany.

E-mail: Martin_Brehm@gmx.de

Computational Details

In order to validate the methodology, three different molecular dynamics simulations of different systems were prepared – see Table 1.

For the bulk phase system (uracil in water), one molecule Uracil and 32 molecules Water were placed inside a cubic simulation cell with the Packmol software.[1] After 1 ns of pre-equilibration using the LAMMPS program package[2] in the NpT ensemble, using the OPLS–AA force field[3] for Uracil and the TIP4P–EW force field for water,[4] a density of 0.999 $\mathrm{g\,cm^{-1}}$ resulted. An *ab initio* molecular dynamics simulation was set up from the final structure. For the two gas phase systems, the steps described above were skipped.

Table 1: Simulated system details.

System	**Ingredients**	**Cell Vector (pm)**	**Density ($\mathrm{g\,cm^{-1}}$)**
Uracil (Water)	1 Uracil 32 Water	1045.8	0.999
Uracil (Vacuum)	1 Uracil	1000.0	0.186
o-Nitrophenol (Vacuum)	1 *o*-Nitrophenol	1000.0	0.231

For the BOMD simulations, we used the program package CP2k,[5] employing the Quickstep method[6] and orbital transformation[7] / DIIS for fast convergence. The electronic structure was calculated with density functional theory,[8,9] utilizing the BLYP functional[10,11] together with the recent reparametrization[12] of Grimme's D3 dispersion correction[13] with Becke–Johnson damping. Basis sets of the kind MOLOPT-DZVP-SR-GTH[14] and GTH pseudopotentials[15,16] were applied to all atoms. The plane wave cutoff was set to 280 Ry, and an SCF convergence criterion of 10^{-6} was used. The time step was chosen to be 0.5 fs in all simulations. The simulation temperature was adjusted to 300 K by a Nosé–Hoover thermostat chain[17–19] (*i. e.*, NVT ensemble). After two more equilibration intervals (1 ps with massive thermostating and thermostat time constant $\tau = 10$ fs, then 30 ps with global thermostating and thermostat time constant $\tau = 100$ fs), a production run with the thermostat settings of the latter equilibration interval was performed for 20.0 ps (*i. e.*, 40 000 time steps).

From the BOMD production trajectories, snapshots were taken every 2.5 fs (*i. e.*, every 5 steps), so that 8 000 snapshots per system resulted. For each of these snapshots, a real-time propagation run (RTP) was started with CP2k. The initial wave function for the propagation was optimized under the influence of an external periodic electric field in X, Y, and Z direction. For each field direction, a separate RTP run was performed. The absolute value of the electric field amounted to $|\mathbf{E}| = 5.0 \cdot 10^{-4}$ a.u. $= 2.57 \cdot 10^{8}\,\mathrm{V\,m^{-1}}$. Directly in the beginning of the RTP runs, the electric field was switched off (step response). The propagation time step was set to 0.0125 fs, and 1 280 steps were performed (*i. e.*, 16 fs of total physical time). In the RTP runs, we chose EPS_DEFAULT to 10^{-10} and EPS_ITER to 10^{-6}. Every 0.0625 fs (*i. e.*, every 5 propagation steps), the total electron density was written to disk in Gaussian CUBE file format, so that 256 frames per BOMD snapshot resulted. The spatial resolution of the volumetric grid was $108 \times 108 \times 108$ for all three systems. The CUBE files were compressed to BQB format[20] directly after each RTP run. The computational cost was 1 350 core hours for the BOMD production run, 230 000 core hours for the RTP runs, and 430 core hours for compressing the electron density and performing the Voronoi integration.

In each of the volumetric frames, molecular electric dipole moments $\boldsymbol{\mu}$ were computed by integrating over the electron density $\rho(\mathbf{r})$, using our Voronoi integration technique[21] with van-der-Waals atom radii for the radical Voronoi tessellation:

$$\boldsymbol{\mu} = \sum_{n=1}^{N_{\mathrm{Mol}}} q_n \mathbf{r}_n - \int_{\mathrm{Mol}} \rho(\mathbf{r})\, \mathbf{r}\, d^3\mathbf{r}, \tag{1}$$

where q_n denotes the nuclear charge of atom n, and N_{Mol} the number of atoms within the selected molecule. From the molecular dipole time series, the dynamic polarizability tensors were computed according to Equation 1 in the main manuscript. A value of $c = 7.0$ for the constant in the Gaussian window function was applied. In the Fourier transform to obtain the Raman invariants (Equations 2 and 3 in the main manuscript), an autocorrelation depth of 5.12 ps and a Hann window function ($\cos^2$) were applied.

Complex Autocorrelation

Following from the definition of autocorrelation $\langle f(\tau) \cdot f(\tau + t) \rangle_\tau = \int f(\tau + t) \cdot \overline{f(\tau)} \mathrm{d}\tau$, the autocorrelation of a complex time series $f(t)$ can be computed from autocorrelations and cross-correlations of real time series in the following way:

$$\begin{aligned} \Big\langle f(t) \cdot f(t+\tau) \Big\rangle_\tau = &\Big\langle \mathrm{Re}\big(f(t)\big) \cdot \mathrm{Re}\big(f(t+\tau)\big) \Big\rangle_\tau + \Big\langle \mathrm{Im}\big(f(t)\big) \cdot \mathrm{Im}\big(f(t+\tau)\big) \Big\rangle_\tau \\ &+ i \left[\Big\langle \mathrm{Re}\big(f(t)\big) \cdot \mathrm{Im}\big(f(t+\tau)\big) \Big\rangle_\tau - \Big\langle \mathrm{Im}\big(f(t)\big) \cdot \mathrm{Re}\big(f(t+\tau)\big) \Big\rangle_\tau \right] \end{aligned} \tag{2}$$

Dynamic Polarizability

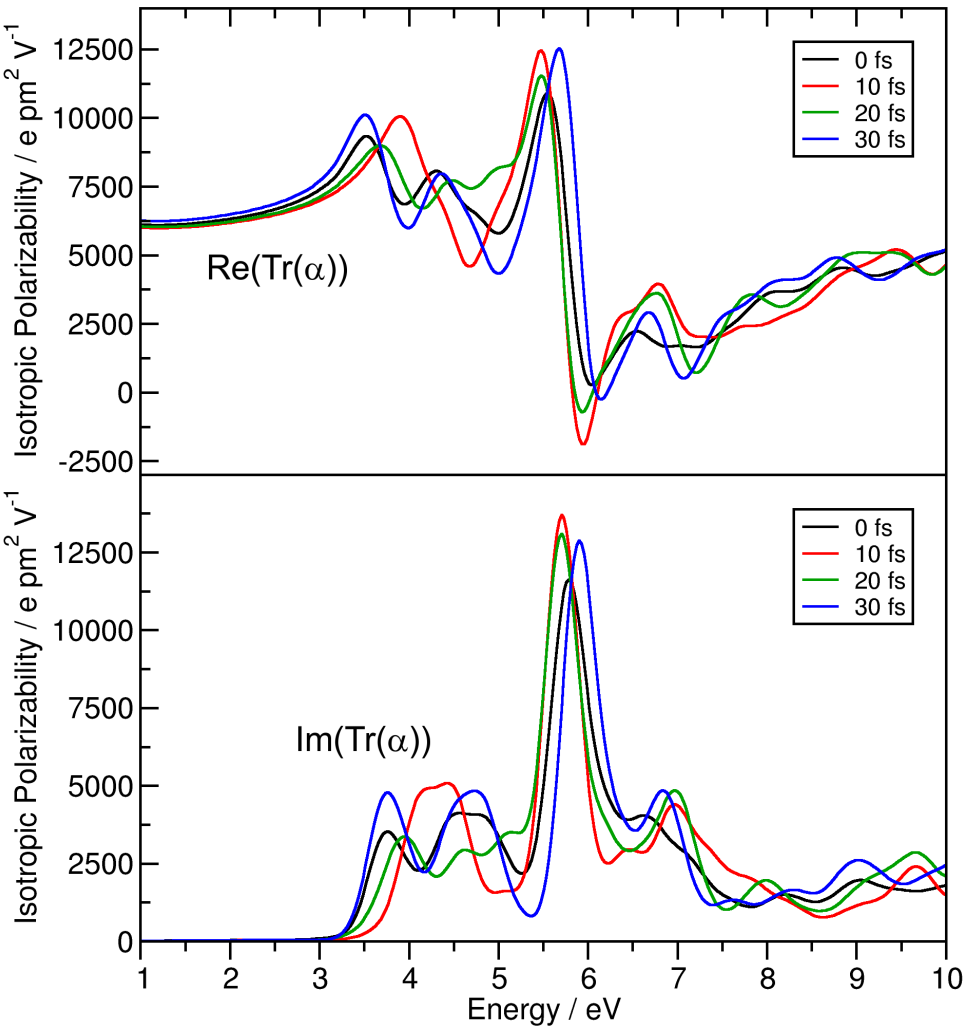

Figure S1: Real part *(upper panel)* and imaginary part *(lower panel)* of the computed isotropic dynamic polarizability of the uracil molecule in four different snapshots of the uracil in water simulation.

Full Range Spectra

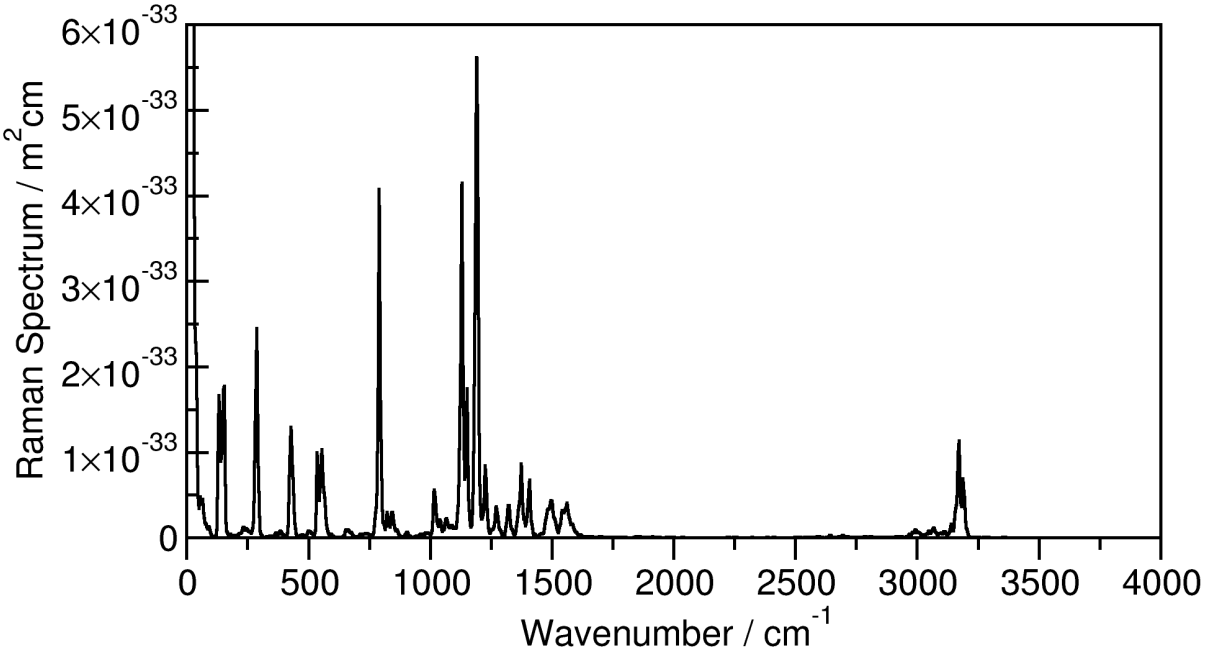

Figure S2: AIMD-based non-resonant Raman spectrum of *ortho*-nitrophenol in gas phase (at 1.17 eV / 1060 nm).

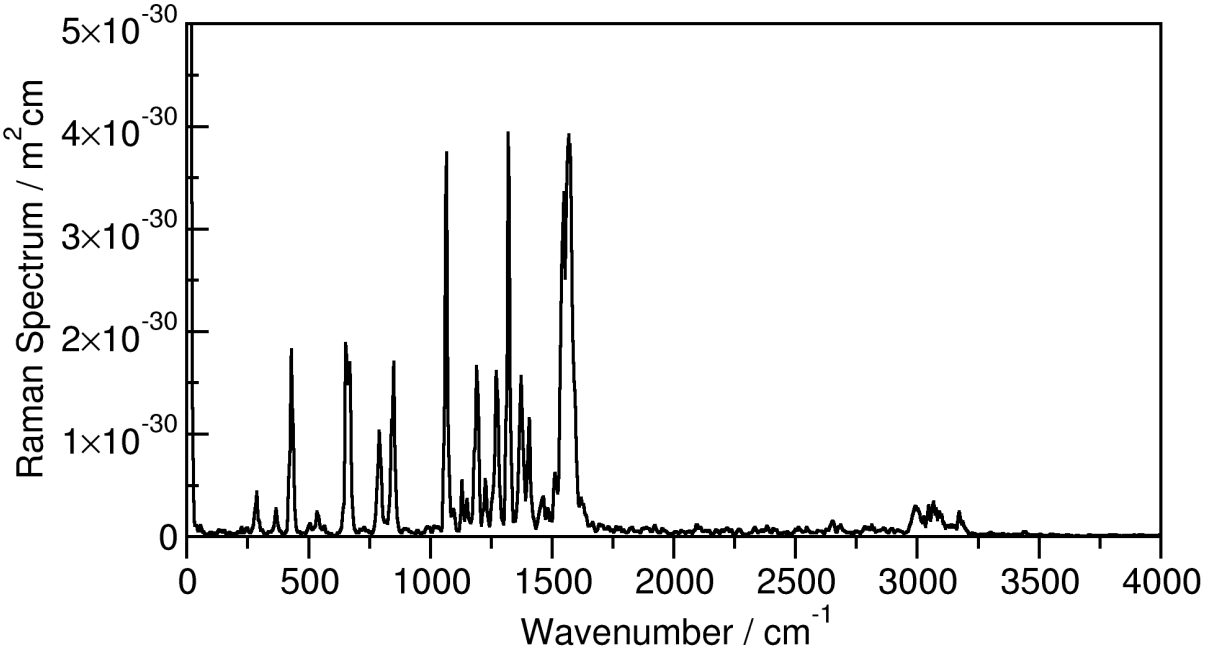

Figure S3: AIMD-based resonance Raman spectrum of *ortho*-nitrophenol in gas phase (at 2.80 eV / 443 nm).

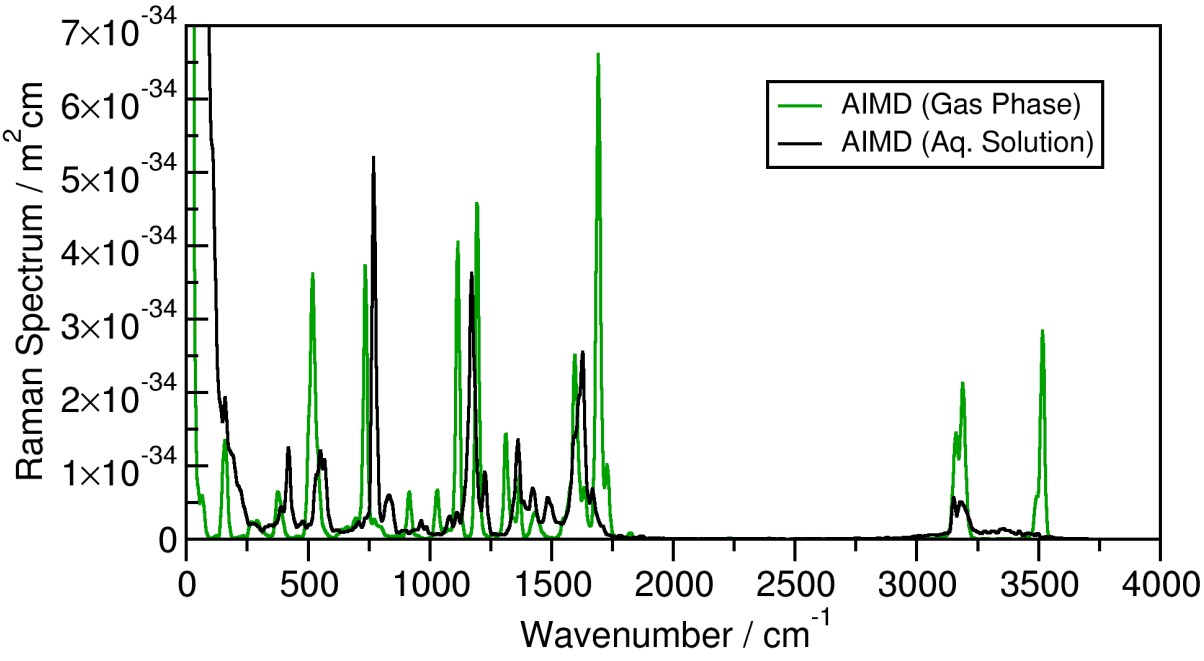

Figure S4: AIMD-based non-resonant Raman spectra of uracil in gas phase *(green curve)* and aqueous solution *(black curve)* at 1.17 eV / 1060 nm.

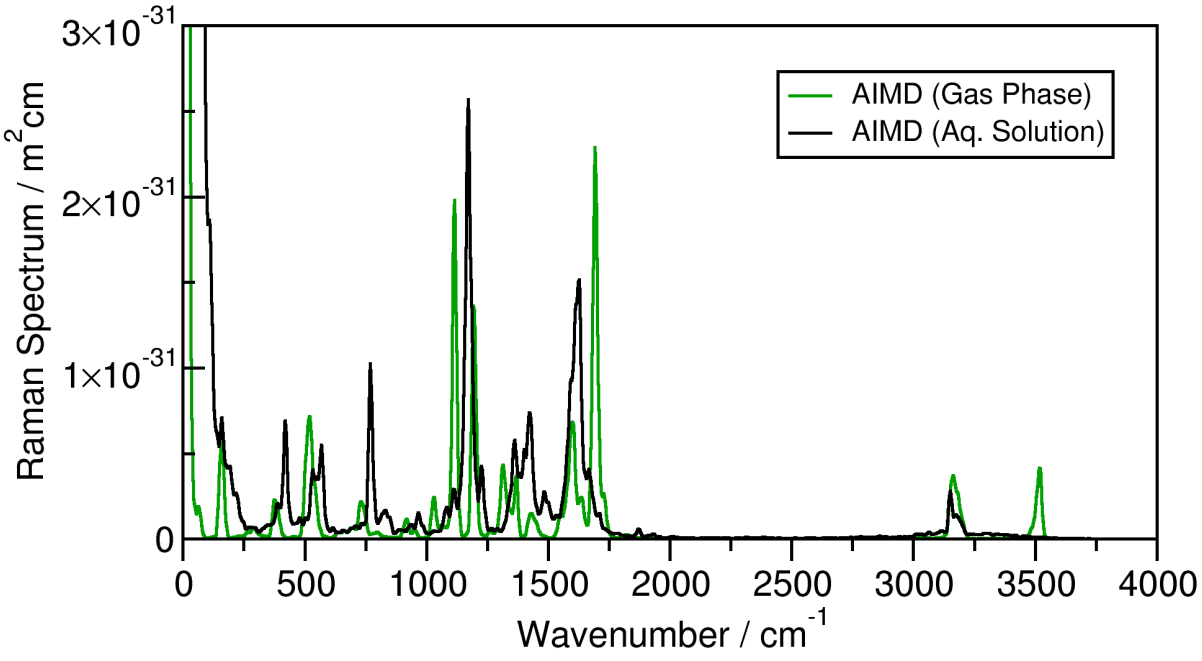

Figure S5: AIMD-based resonance Raman spectra of uracil in gas phase *(green curve)* and aqueous solution *(black curve)* at 3.65 eV / 340 nm.

ortho-Nitrophenol

As a second model system, we simulated *ortho*-nitrophenol in gas phase, as it has been investigated by previous computational studies[22,23] on the resonance Raman effect which were not based on molecular dynamics simulations. We compare both the non-resonant as well as the resonant Raman spectra from our approach with the results from a static calculation[23] in the upper panel of Figure S6. As expected, there are some differences because the AIMD-based spectra take into account some anharmonic effects which are completely missing in the static spectra. This leads both to shifts in band positions and to line broadening which alters the peak heights. Apart from these effects, we find that the change in relative band intensities and the total increase in intensity due to the resonance Raman effect is captured by our approach very well.

As explained above, our method does not require a set of laser energies as input, but yields the resonance Raman spectra for all possible laser energies in one pass. In the lower panel of Figure S6, we present the set of all such spectra, with the laser energy on the ordinate axis, and the vibrational frequency shown on the abscissa. Each spectrum (*i. e.*, each row of the plot) has been normalized to uniform maximum band height, because otherwise the non-resonant spectra would not be visible at all due to the strong increase in intensity caused by the resonance Raman effect. It is clearly visible how bands which are almost invisible in the non-resonant Raman spectrum become very intense at certain laser energies (*e. g.*, the bands at 850, 1050, and 1600 cm^{-1}). Such an increase in intensity only happens if the spectral band involves movement of atoms which take part in the electronic excitation at a given laser energy.

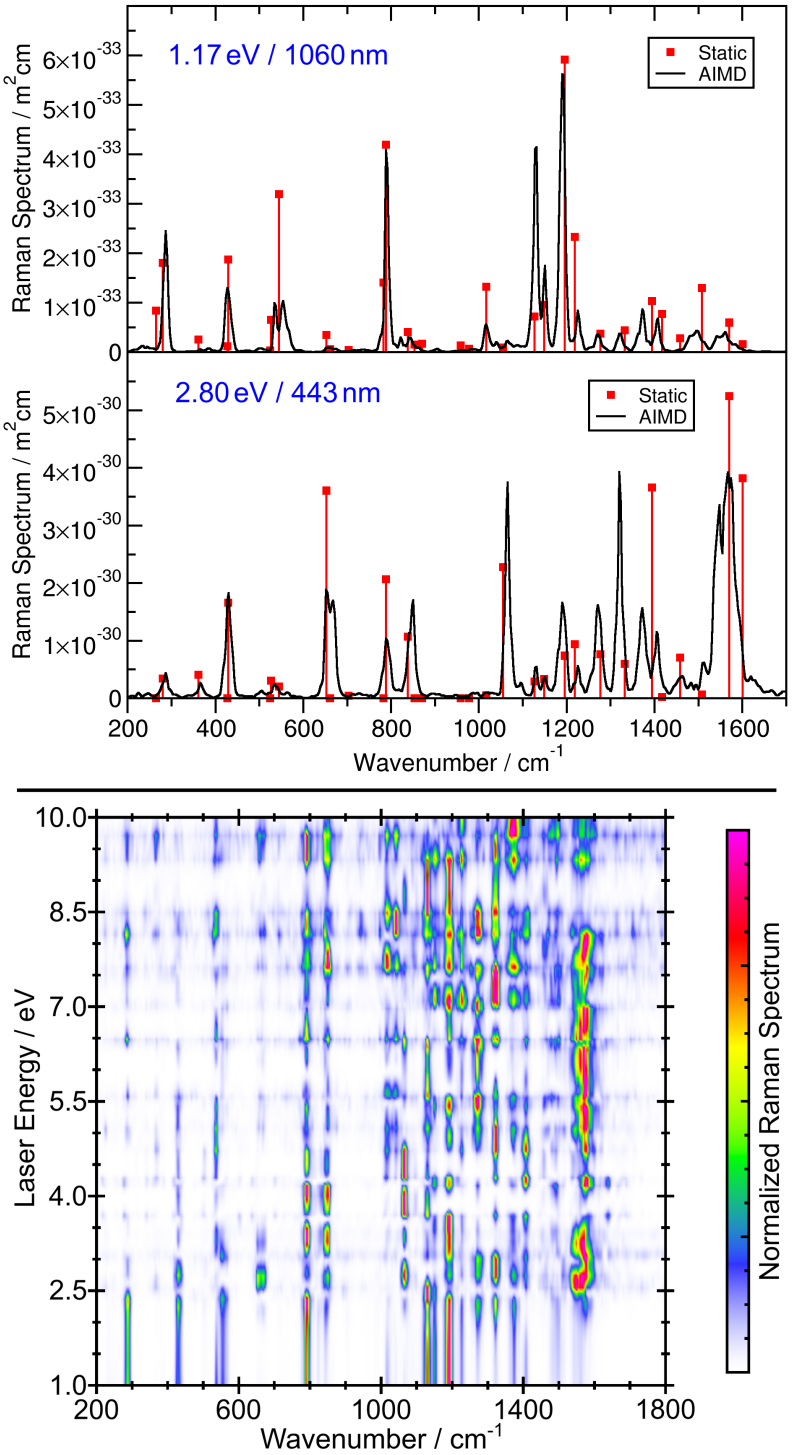

Figure S6: Upper panel: AIMD-based resonance Raman spectrum of *o*-nitrophenol *(black curve)* compared to results from static calculation[23] *(red bars)* for two different laser energies; Lower panel: AIMD-based resonance Raman spectra of *o*-nitrophenol over a wide range of laser energies (normalized).

References

(1) Martínez, L.; Andrade, R.; Birgin, E. G.; Martínez, J. M. PACKMOL: A Package for Building Initial Configurations for Molecular Dynamics Simulations. *J. Comp. Chem.* **2009**, *30*, 2157–2164.

(2) Plimpton, S. Fast Parallel Algorithms for Short-Range Molecular Dynamics. *J Comp Phys* **1995**, *117*, 1–19.

(3) Kaminski, G. A.; Friesner, R. A.; Tirado-Rives, J.; Jorgensen, W. L. Evaluation and Reparametrization of the OPLS-AA Force Field for Proteins Via Comparison with Accurate Quantum Chemical Calculations on Peptides. *J. Phys. Chem. B* **2001**, *105*, 6474–6487.

(4) Horn, H. W.; Swope, W. C.; Pitera, J. W.; Madura, J. D.; Dick, T. J.; Hura, G. L.; Head-Gordon, T. Development of an Improved Four-Site Water Model for Biomolecular Simulations: TIP4P-EW. *J. Chem. Phys.* **2004**, *120*, 9665–9678.

(5) Hutter, J.; Iannuzzi, M.; Schiffmann, F.; Vandevondele, J. CP2k: Atomistic Simulations of Condensed Matter Systems. *Wiley Interdiscip. Rev.: Comput. Mol. Sci.* **2014**, *4*, 15–25.

(6) Vandevondele, J.; Krack, M.; Mohamed, F.; Parrinello, M.; Chassaing, T.; Hutter, J. Quickstep: Fast and Accurate Density Functional Calculations Using a Mixed Gaussian and Plane Waves Approach. *Comput. Phys. Commun.* **2005**, *167*, 103–128.

(7) Vandevondele, J.; Hutter, J. An Efficient Orbital Transformation Method for Electronic Structure Calculations. *J. Chem. Phys.* **2003**, *118*, 4365–4369.

(8) Hohenberg, P.; Kohn, W. Inhomogeneous Electron Gas. *Phys. Rev. B* **1964**, *136*, 864.

(9) Kohn, W.; Sham, L. Self-Consistent Equations Including Exchange and Correlation Effect. *Phys. Rev.* **1965**, *140*, 1133.

(10) Becke, A. Density-Functional Exchange-Energy Approximation with Correct Asymptotic Behavior. *Phys. Rev. A* **1988**, *38*, 3098–3100.

(11) Lee, C.; Yang, W.; Parr, R. Development of the Colle-Salvetti Correlation Energy Formula into a Functional of the Electron Density. *Phys. Rev. B* **1988**, *37*, 785–789.

(12) Smith, D. G. A.; Burns, L. A.; Patkowski, K.; Sherrill, C. D. Revised Damping Parameters for the D3 Dispersion Correction to Density Functional Theory. *J. Phys. Chem. Lett.* **2016**, *7*, 2197–2203.

(13) Grimme, S.; Antony, J.; Ehrlich, S.; Krieg, S. A Consistent and Accurate Ab Initio Parametrization of Density Functional Dispersion Correction (DFT-D) for the 94 Elements H-Pu. *J. Chem. Phys.* **2010**, *132*, 154104.

(14) Vandevondele, J.; Hutter, J. Gaussian Basis Sets for Accurate Calculations on Molecular Systems in Gas and Condensed Phases. *J. Chem. Phys.* **2007**, *127*, 114105.

(15) Goedecker, S.; Teter, M.; Hutter, J. Separable Dual-Space Gaussian Pseudopotentials. *Phys. Rev. B* **1996**, *54*, 1703–1710.

(16) Hartwigsen, C.; Goedecker, S.; Hutter, J. Relativistic Separable Dual-Space Gaussian Pseudopotentials from H to Rn. *Phys. Rev. B* **1998**, *58*, 3641–3662.

(17) Nose, S. A Unified Formulation of the Constant Temperature Molecular Dynamics Methods. *J. Chem. Phys.* **1984**, *81*, 511–519.

(18) Nose, S. A Molecular Dynamics Method for Simulations in the Canonical Ensemble. *Mol. Phys.* **1984**, *52*, 255–268.

(19) Martyna, G.; Klein, M.; Tuckerman, M. Nosé–Hoover Chains: The Canonical Ensemble via Continuous Dynamics. *J. Chem. Phys.* **1992**, *97*, 2635–2643.

(20) Brehm, M.; Thomas, M. An Efficient Lossless Compression Algorithm for Trajectories of Atom Positions and Volumetric Data. *J. Chem. Inf. Model.* **2018**, *58*, 2092–2107.

(21) Thomas, M.; Brehm, M.; Kirchner, B. Voronoi Dipole Moments for the Simulation of Bulk Phase Vibrational Spectra. *Phys. Chem. Chem. Phys.* **2015**, *17*, 3207–3213.

(22) Guthmuller, J. Assessment of TD-DFT and CC2 Methods for the Calculation of Resonance Raman Intensities: Application to o-Nitrophenol. *J. Chem. Theor. Comput.* **2011**, *7*, 1082–1089.

(23) Thomas, M.; Latorre, F.; Marquetand, P. Resonance Raman Spectra of ortho-Nitrophenol Calculated by Real-Time Time-Dependent Density Functional Theory. *J. Chem. Phys.* **2013**, *138*, 044101.